International Journal of Advanced Research in Biological Sciences
ISSN: 2348-8069
www.ijarbs.com
Volume 3, Issue 6 - 2016

Research Article

SOI: http://s-o-i.org/1.15/ijarbs-2016-3-6-34

Coordination behaviour and biological activity of Co(II), Ni(II) and Cu(II) complexes of phenyl indandionepyridyl thiosemicarbazone ligand.

Ola A. El-Gammal[1], Ibrahim M. El-Mehasseb[2], Raghda H. Salama[1], Gaber M. Abu El-Reash[1*]

[1]Department of Chemistry, Faculty of Science, Mansoura University, Mansoura, Egypt.
[2]Department of Chemistry, Faculty of Science, Kafr El-Sheikh University, Kafr El-Sheikh, Egypt.
*** Corresponding author.: Prof.Dr.Gaber Mohammed Abu El-Ereash**
Tel.: +201000373155; fax: +20 502219214.
E-mail: *gaelreash@mans.edu.eg*

Abstract

Co(II), Ni(II) and Cu(II) complexes derived from hydrazone ligand HIPT) prepared via the condensation of 4-(2-pyridyl)-3-thiosemicarbazide in a 1:1 molar ratio with 2-phenyl-1H-indene-1,3(2H)-dione were synthesised and characterized using elemental analysis, magnetic and spectral measurements. The proposed structures of both complexes were proved using DFT optimization and conformational analysis. The thermal decomposition behaviour of complexes were discussed. Kinetic parameters (ΔH, ΔS, ΔG, E and A) of resulted thermal decomposition stages have been calculated using Coats-Redfern and Horowitz-Metzger methods. Co(II) complex shows potent antioxidant activity and moderate Cytotoxicity activity. On the other hand, Co(II) complex has no activity against *Staphylococcus aureus, Escherichia coli* and *Candida albicans*

Keywords: Hydrazones; Spectral characterization; thermal degradation; antibacterial, antioxidant; Cytotoxicity activity.

Introduction

The thiosemicarbazones derivatives which contains the tautomer (C=S) thione and (=C-S) thiolmoieties played an important rolein the coordination chemistry because of their chelating capability towards transition metal ions [1]. The Schiff base ligands with sulphur in the presence of additional active centers such as oxygen and nitrogen they readily form stable complexes contains NOS, NNS or NS donors [2-5]. A number of reports concerning thiosemicarbazones and their metal complexes were established owing to their chemical and biological activities [6-10]. Actually, some thiosemicarbazones of NNS donors possess carciostatic potency[11] and oversize in *vivo* activity against several human tumor lines [12, 13] but in some cases, the structural changes which belong to the availability to coordination may destroy or reduce its medicinal values [14].The present work aims to formation and investigation of Co(II), Ni(II) and Cu(II) complexes of (E)-2-(3-oxo-2-phenyl-2,3-dihydro-1H-inden-1 - ylidene) - N- (pyridin-2-yl)hydrazine-1-carbothioamide (HIPT). The chelation behavior and the geometry of complexes are discussed based on the resulted (DFT) quantum calculations, the magnetic moment and the different spectroscopic methods (^{1}H and ^{13}C-NMR, IR, UV-visible).

Moreover, the kinetics and thermodynamic characteristics of the thermal decomposition steps have been evaluated employing Coats–Redfern and Horowitz–Metzger models. Also, their anti-bacterial, antioxidant and Cytotoxicity assay have been tested.

Experimental

Materials and Instrumentation.

The Co(II), Ni(II)and Cu(II) chloride salts, 2-amino pyridine, methyl iodide, carbon disulfide, hydrazine hydrate and with 2-phenyl-1H-indene-1,3(2H)-dione were of analytical grade. (C, H, S and N) percent in the prepared HIPT and complexes were detected using a Perkin–Elmer 2400 series II analyzer, while metal and chloride contents were carried out according to the standard methods[15]. Thermogravimetric (TGA) and differential thermal analysis (DTA) measurements were carried out on a Shimadzu TGA-50H thermogravimetric analyzer at temperature range (20–800^{o}C) with a heating rate of 10 ^{o}C/min and nitrogen flow rate of 15 ml/min. The standard used in the experiment is Pt. 10% Rh. A Sherwood Magnetic Balance was utilized to measure the magnetic susceptibility of solid complexes.IR spectra were recorded on a Mattson 5000 FTIR spectrophotometer in range (4000–400 cm^{-1}) using KBr discs, while Perkin Elmer Lamda 25 UV/Vis Spectrophotometer was used to record the electronic spectra of complexes in DMSO solution.^{1}H and ^{13}C-NMR measurements in d_6-DMSO at room temperature were carried out on Mercury and Gemini 400 MHZ spectrometer.

Synthesis of HIPT

4-(2-pyridyl)-3-thiosemicarbazide was synthesized according to the general literature method [16]. HIPT was prepared by mixing 4-(2-pyridyl)-3-thiosemicarbazide in a 1:1 molar ratio with 2-phenyl-1H-indene-1,3(2H)-dione in a hot ethanolic solution. The reaction mixture was boiled under reflux for 3 h. The isolated compound was filtered off, recrystallized from absolute ethanol and finally dried in a vacuum desiccator over anhydrous calcium chloride.

Synthesis of Complexes

A hot ethanolic solution of the respective metal chloride (1.0 mmol) was added to a hotethanolic medium of HIPT(0.372 g, 1.0mmol). The resultant mixture was boiled under reflux for 3– 4 h. All complexes were filtered off, then washed well with hot EtOH followed by diethyl ether and dried over anhydrous $CaCl_2$in a vacuum desiccator. The physical and analytical data are listed in (Table 1). It is clear that, prepared complexes are stable in air and have high melting points.

Table 1. Analytical and physical data of H_2STH and its complexes.

Compound molecular formula	(F.Wt)	color	M.P. (^{o}C)	Found (calcd.)% M	Cl	C	H	N	S	yield %
HIPT		Paige	183	—	—	67.25	4.27	15.47	8.25	95
$C_{21}H_{16}N_4OS$	372.45					(67.72)	(4.33)	(15.04)	(8.61)	
[Co(IPT)Cl].(H_2O)		green	245	12.52	7.16	52.21	3.65	11.36	6.85	87
$C_{21}H_{17}ClCoN_4O_2S$	483.84			(12.18)	(7.33)	(52.13)	(3.54)	(11.58)	(6.63)	
[$Ni(IPT)_2$]		yellowish brown	235	7.65	—	62.78	3.44	13.53	8.47	78
$C_{42}H_{30}NiN_8O_2S_2$	801.57			(7.32)		(62.93)	(3.77)	(13.98)	(8.00)	
[Cu(HIPT)Cl_2(H_2O)].H_2O		reddish brown	227	11.74	13.29	46.89	3.33	10.65	5.74	88
$C_{21}H_{20}Cl_2CuN_4O_3S$	542.93			(11.70)	(13.06)	(46.46)	(3.71)	(10.32)	(5.91)	

Biology

Antibacterial activity

The concerned ligand and its complexes were individually tested against a panel of gram positive *Staphylococcus aureus*, negative *Escherichia coli* bacterial and *Candida albicans*. To evaluated the efficiency of compounds under study, the same tests carried out on the standard antibiotic ampicillin and antifungal colitrimazole. The procedure of treatment and evaluation were carried out according to the standard methods[17]. The % efficiency index for each compound was calculated by the mathematic formula as below:

$$\%\,Activity\ Index = \frac{Zone\ of\ inhibition\ by\ test\ compound\ (diametre)}{Zone\ of\ inhibition\ by\ standard\ (diametre)} x\ 100$$

Anti-Oxidant Assays by ABTS Method:

The tests and procedure steps of treatment were carried out as described in the literature. L –ascorbic acid was used as standard antioxidant (Positive control) [18-20].

Cytotoxicity assay

Materials and methods

Cell line

Heptacelluar carcinoma (HepG2) and human prostate cancer cell line (PC3) were obtained from ATCC via Holding company for biological products and vaccines (VACSERA), Cairo, Egypt.

Chemical reagents

The reagents RPMI-1640 medium, MTT, DMSO and 5-fluorouracil (sigma co., St. Louis, USA), Fetal Bovine serum (GIBCO, UK). 5-fluorouracil was used as a standard anticancer drug for comparison.

MTT assay

The MTT assay is carried out to evaluate the inhibitory efficiency on the cell growth as described in the literature [21, 22].

$$\text{The relative cell viability\%} = \frac{A_{570} \text{ of Treated Samples}}{A_{570} \text{ of Untreated Samples}} \times 100$$

Molecular Modeling

DMOL^3 program used to study the cluster calculations [23] in Materials Studio package [24].Density functional theory DFT semi-core pseudopods calculations (dspp) were done using the double numerical basis sets plus polarization functional (DNP). The DNP basis sets are of comparable quality to 6-31G Gaussian basis sets [25]. It was reported previously by Delley et al. that Gaussian basis sets are less accurate than the DNP basis sets of the same size [26]. The RPBE functional is employed to take account of the exchange and correlation effects of electrons , where it is so far considered the best exchange–correlation functional [27]based on the generalized gradient approximation (GGA) [28]. The geometric optimization displayed without any symmetry limitation.

Results and Discussion

IR Spectra of HIPT and Complexes.

Three orientation (A, B and C) are possible for the tautomerism of ligand. For such ligand, the result of quantum calculations led to three values of minimum energy conformations (Structure 1) within energy differences of less than 0.05 Kcal/mol. So, it is clear from the calculations that the conformer (B) is more stable than (A) and (C) with energy content of -4979.08, -4979.03and -4966.05 Kcal/mol, respectively.

Principle of bands for HIPT and its complexes depending on carful comparison are presented in table 2. The IR spectrum of HIPT (structure 2) exhibits four bands at 1720, 1634, 1602 and 852 cm^{-1} which are assigned to ν(C=O), ν(C=N)$_{azomethine}$, [ν(C=C)$_{phenyl}$ and ν(C=N)$_{pyridyl}$] and ν(C=S) of thione group, respectively[29-31]. Also, the spectrum shows two bands at 3200 and 3162 cm^{-1} due to ν(NH)$_{asym}$ and ν(NH)$_{sym}$, respectively. Moreover, the bands at 992 and 637 cm^{-1} attributed to ν(N-N) [32] and δ(C=N)$_{py}$ which are shifted to higher frequencies upon complexation.

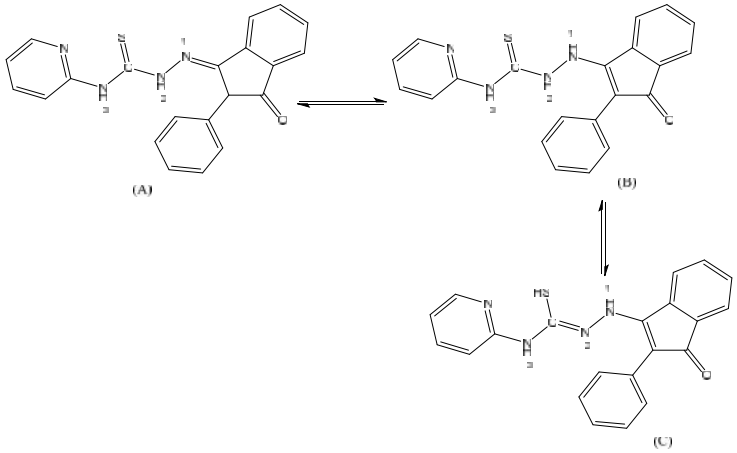

Structure 1

Table 2. Assignments of IR spectral bands of HIPT and its complexes.

Compound	N (C=O)	Y (C=N) azo	N (C=N) py	Y (NH) sym	N (NH) asym	Y (C=N) *	υ/ δ (C=S)	N (N-N)	Δ (C=N) py	N (M-O)	N (M-N)
HIPT	1720	1634	1602	3162	3200	-	1432, 852	992	637	-	-
$[Co(IPT)Cl].H_2O$	1730	1606	1509	-	3230	1639	-, 919	1051	674	-	464
$[Ni(IPT)_2]$	1725	1605	1516	-	3201	1647	-, 910	1052	675	-	420
$[Cu(HIPT)Cl_2(H_2O)].H_2O$	1736	1620	1504	3186	3218	-	1421, 903	1013	673	520	492

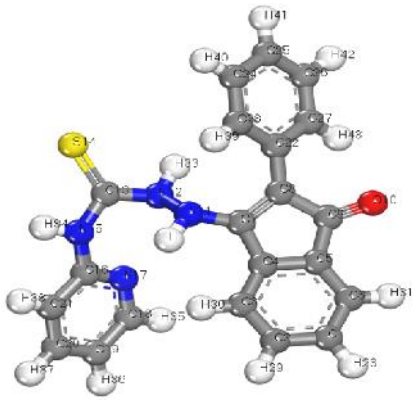

Structure 2.Molecular modeling of HIPT

HIPT act as neutral tridentate ligand via (C=N) of both azomethine and pyridyl ring as well as the sulfur of thione moiety. This behavior is found in Cu(II) complex (structure 3) and is suggested by:

(i) The shift of both $\nu(C=N)_{pyridyl}$ and $\nu(C=N)_{azomethine}$to lower wave number [33].
(ii) The clear change in both position and intensity of thio-amide IR bands [34].
(iii) The appearance of (NH) bands around its original position.

Also, HIPT behaves in Co(II) and Ni(II) complexes (structures 4 and 5) as mono-negative tridentate via the sulfur of (C-S) in thiol form with deprotonation and both $(C=N)_{py}$ and $(C=N)_{azomethine}$ groups. This behavior is suggested by:

(i) The synchronism of appearance of new viberations due to (C=N) and (C-S) with disappearance viberations due to NH and C=S moieties[34].
(ii) The shift of both $\nu(C=N)_{py}$ and $\nu(C=N)_{azomethine}$to lower wavelengths [33].

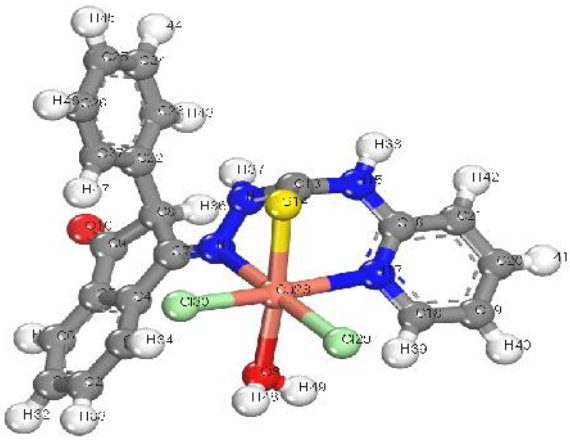

Structure 3.Molecular modeling of $[Cu(HIPT)Cl_2(H_2O)].H_2O$

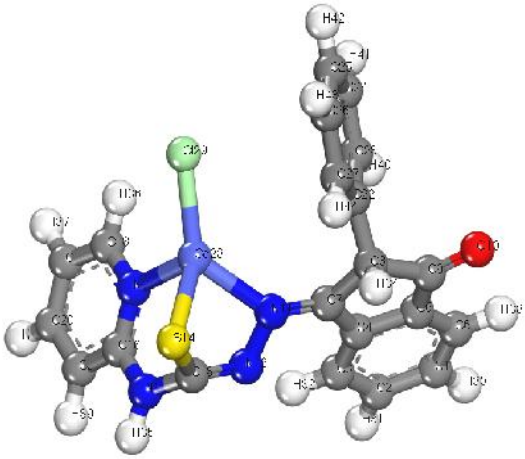

Structure 4.Molecular modeling of $[Co(IPT)Cl].H_2O$

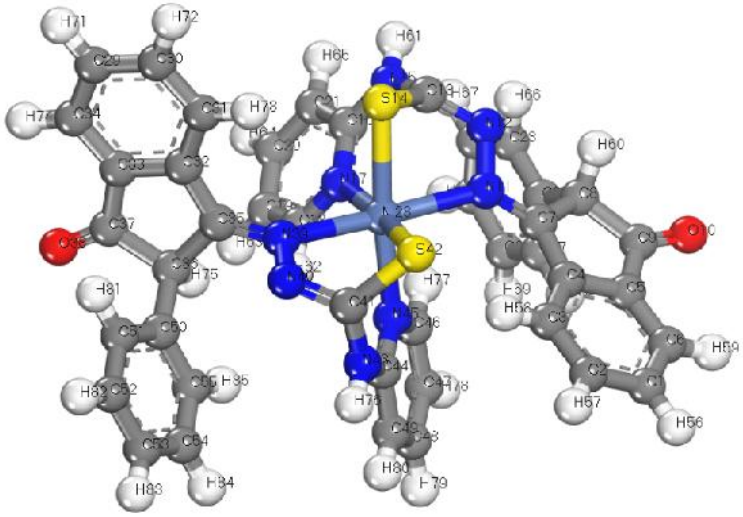

Structure 5.Molecular modeling of $[Ni(IPT)_2]$

^{1}H and ^{13}C-NMR Spectra of the H_2STH.

The ^{1}H-NMR spectrum of HIPT (fig. 1) in d_6-DMSO displayed three signals at δ= 11.03, 7.97 and 4.93 ppm which disappear upon addition of D_2O (fig. 2) (assigned to N^1H, N^3H and N^2H groups. The multi-signals in region 6.96-8.19 ppm corresponding to the (CH) protons in pyridine and benzene rings.

The ^{13}C-NMR (fig. 3) shows four signals at 197.98, 178.52, 153.20 and 152.86 ppm assigned to (CO), (C=S), $(C=N)_{py}$ and $(C=N)_{az.}$ The CH group appeared at 54.29 ppm.

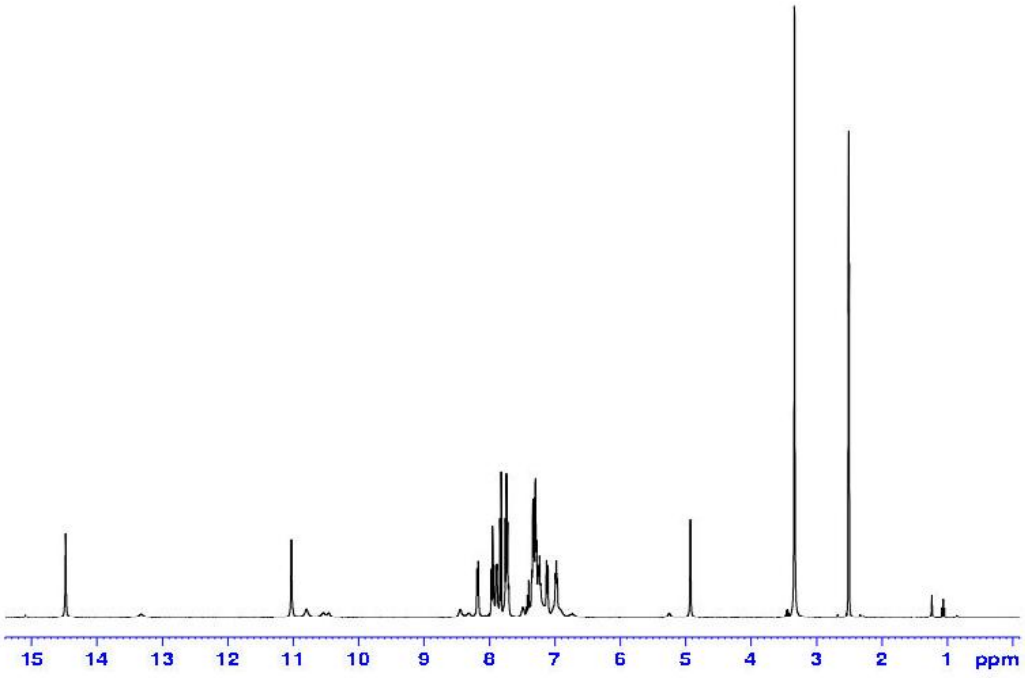

Figure 1: ^{1} HNMR spectra of HIPT.

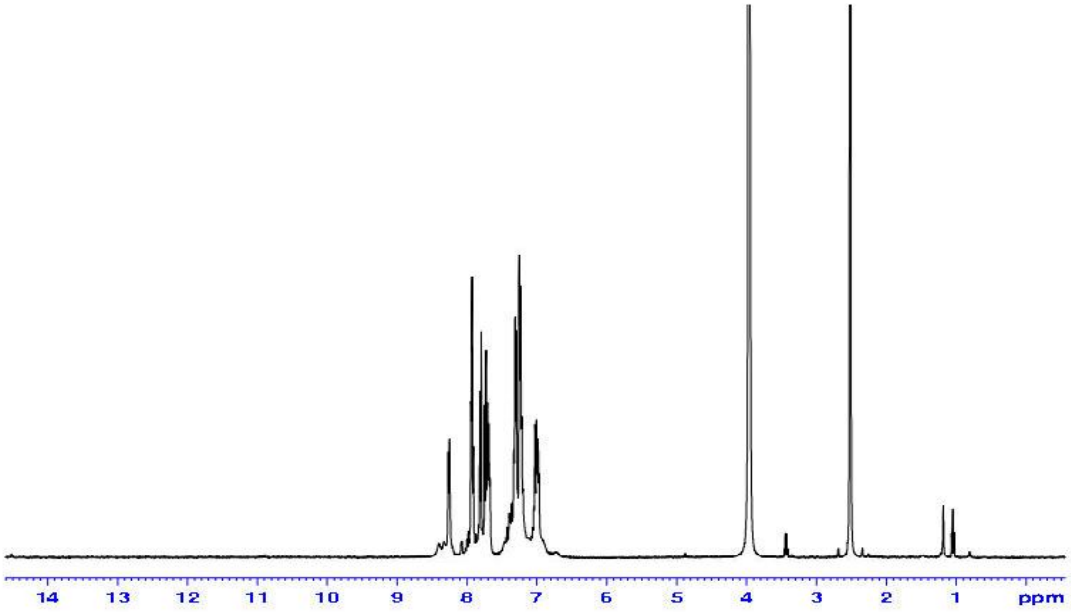

Figure 2: ^{1}HNMR spectra of HIPT with addation of D_2O.

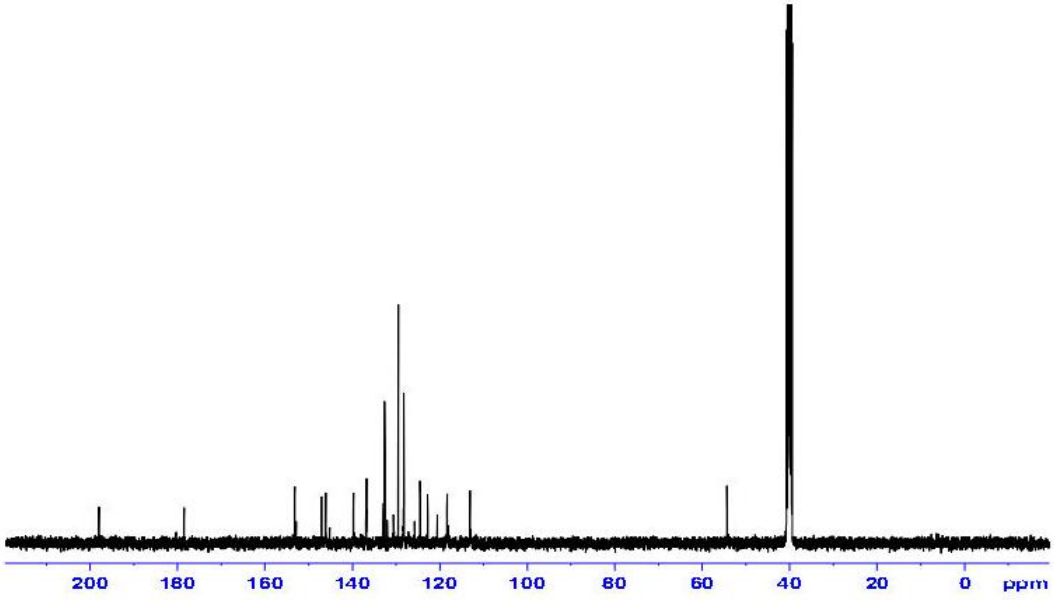

Figure 3: ^{13}CNMR spectra of HIPT.

Magnetic properties and electronic spectra:

The results of the absorption spectra of HIPT and its complexes in DMSO were compiled in table 3. In the spectrum of HIPT the bands at 32258 and 27932 cm^{-1} assignable to ($\pi \rightarrow \pi^{*}$) transition of both (C=O) and (C=N) groups. Also, the bands at 25380 and 22026 cm^{-1} belongs to ($n \rightarrow \pi^{*}$) transition of the same groups [35].

In the spectrum of the [Co(IPT)Cl].H_2O complex, the bands at 21551, 16393 and 14749 cm^{-1} assigned to $^{4}T_2 \rightarrow {}^{4}A_2$, $^{4}T_1(F) \rightarrow {}^{4}A_2$ and $^{4}T_1(P) \rightarrow {}^{4}A_2$ transitions, respectively. The μ_{eff} value (4.36 B.M.) and the color of complex confirmed the tetrahedral geometry of this complex.

The absorption spectrum of $[Ni(IPT)_2]$ complex show one strong band at 2000 cm^{-1} assigned to $^3A_{2g}(F) \rightarrow {}^3T_{1g}(F)(\nu_2)$ and the other weak at 25000 cm^{-1} attributed to $^3A_{2g}(F) \rightarrow {}^3T_{2g}(P)(\nu_3)$ transitions. These transtions reveal that Ni(II) complex possess six coordinate structure and D_4h symmetry. The magnetic moment value, $\mu_{eff.}$=2.77 B.M. reveals the proposed geometry.

The electronic spectrum of Cu (II) complex show d-d transition bands at 22026, 23400 and 25200 cm^{-1}. These spine allowed transitions are attributed to $^2B_{1g} \rightarrow {}^2B_{2g}$ $(d_{x2-y2} \rightarrow d_{xy})$ $(\nu_2)$and $^2B_{1g} \rightarrow {}^2E_g$ $(d_{x2-y2} \rightarrow d_{xz}, d_{yz})$ (ν_3), respectively [36]. These bands indicate that D_4h symmetry and tetragonal geometry of this complex. Moreover, the value of $\mu_{eff.}$ =1.90 B.M. agree with the represented value of d^9system.

Table 3: Electronic spectral data of HIPT and its complexes.

Compound	Band position,cm^{-1}	μ_{eff}(B.M)
HIPT	32258, 27932, 25380, 22026	-
$[Co(IPT)Cl].H_2O$	33557, 32258, 27777, 21511, 16393, 14749	4.36
$[Ni(IPT)_2]$	32467, 25000, 20000	2.77
$[Cu(HIPT)Cl_2(H_2O)].H_2O$	25200, 23400, 22026	1.90

TGA and Dr TGA Studies.

The TG and DTA for solid complexes are depicted inFigs. (4-6). The obtained results approved the proposed formulae. Where, it is clear that the complex decompose in three main stages. The primary stage implies the loss of hydrated water molecules at 50–150^{o}C, followed by the escape of crystalline water at 152–200^{o}C. Then, the sublimation process began at a temperature range of 250–800 ^{o}C and at the end, formation of metal oxide took place.The TGA decomposition steps of water molecules loss with the temperature range and weight loss for the complexes are recorded in table 4.

Table 4: Decomposition steps within the temperature range and weight loss for Co(II), Ni(II) and Cu(II) complexes of HIPT.

Complex	Temp. Range,°C	Removed species	Wt. Loss	
			Found%	Calcd%
$[Co(IPT)Cl].H_2O$	50.37-95.96	$-(H_2O)$	3.81	3.72
	221.33-254.61	-(HCl+ CN)	12.89	12.91
	306.91-382.03	$-(C_5H_4N_2)$	19.28	19.04
	413.41-444.15	-(CN)	4.98	5.38
	531.56-585.77	$-(C_{14}H_{10}S)$	43.86	43.46
	585.77-800.00	CoO(residue)	15.18	15.49
$[Ni(IPT)_2]$	265.46-286.65	$-(N_2+H_2S+H_2O+N_2)$	12.99	13.49
	330.62-389.69	$-(C_{20}H_{14}N_4O)$	40.38	40.71
	463.86-506.77	$-(2(C_6H_6))$	19.70	19.49
	506.77-800.00	$NiS+5C_2$ (residue)	26.93	26.31
$[Cu(HIPT)Cl_2(H_2O)].H_2O$	54.87-150.77	$-(H_2O)$	2.94	3.32
	152.76-193.02	$-(NH_2+H_2O)$	6.19	6.27
	206.92-262.09	$-(Cl_2)$	13.16	13.06
	276.33-350.51	$-(C_6H_4ON)$	19.24	19.54
	392.28-414.90	$-(N_2)$	5.32	5.16
	484.15-670.29	$-(C_{15}H_{10})$	35.60	35.04
	670.29-800.00	CuS (residue)	17.55	17.61

.

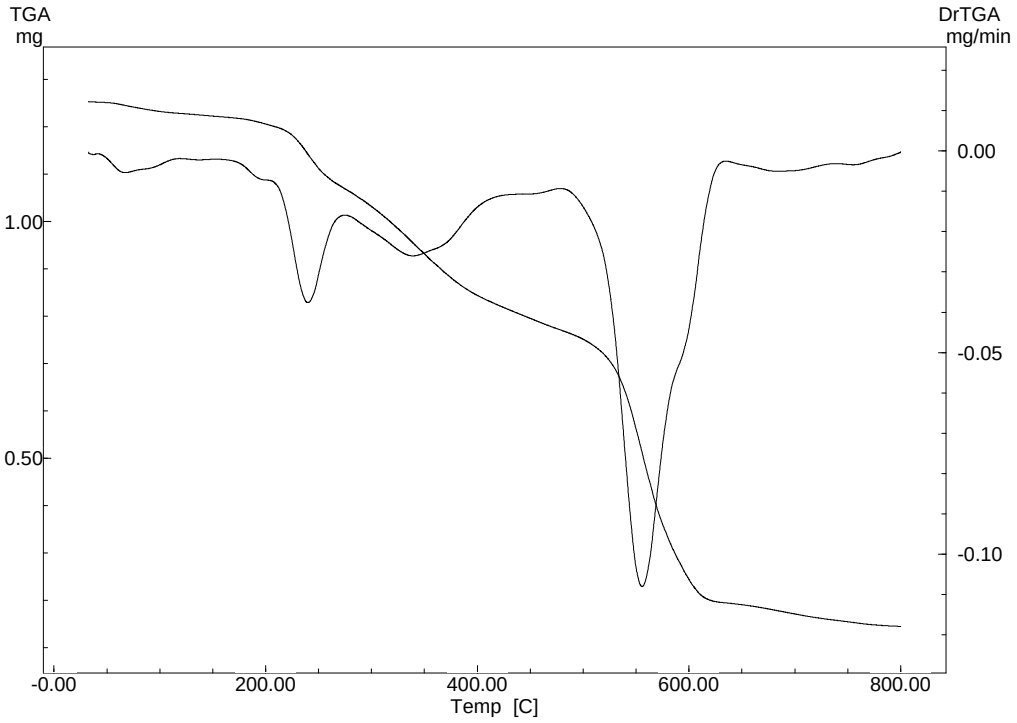

Figure 4: Thermal analysis curves (TGA, DTG) of [Co(IPT)Cl].H_2O Complex.

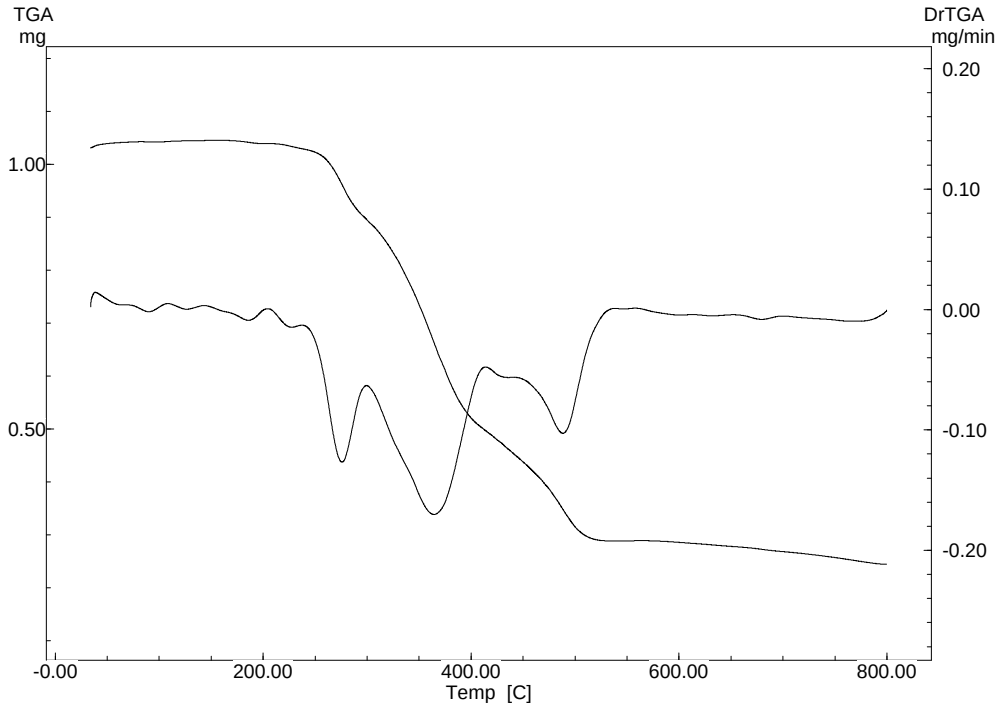

Figure 5: Thermal analysis curves (TGA, DTG) of [$Ni(IPT)_2$] Complex

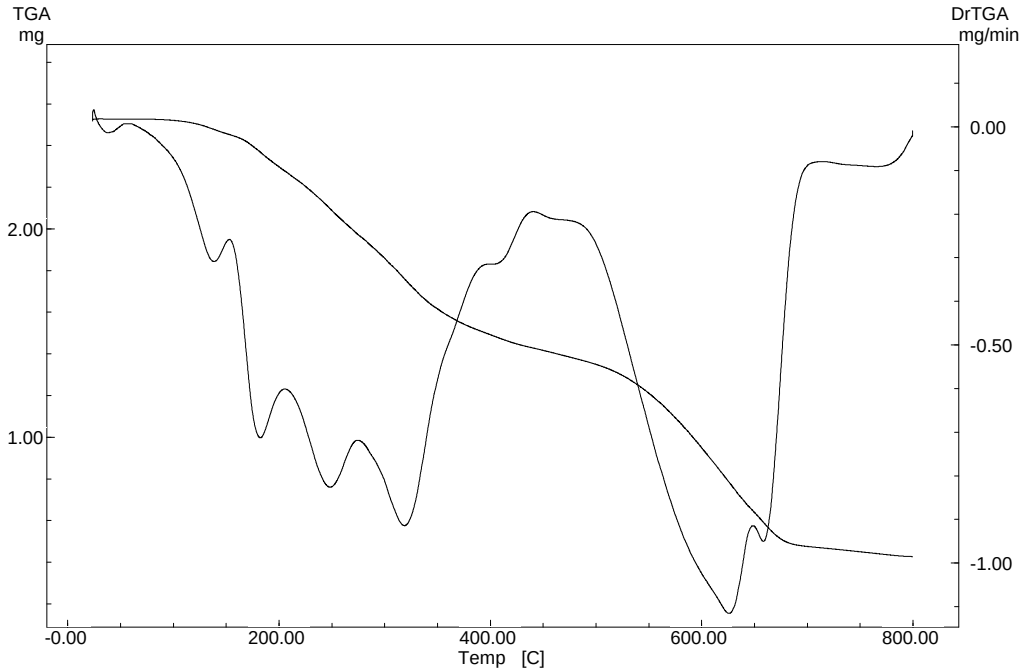

Figure 6: Thermal analysis curves (TGA, DTG) of [Cu(HIPT)Cl_2(H_2O)].H_2O Complex

Kinetic Data of Thermal Degradation:

The kinetic parameters of decomposition stages have been evaluated by using non-isothermal methods. The rate of degradation, dα/dt, is a linear function of rate constant k (temperature dependent) and function of conversion α (temperature independent) and can be expressed as follow [a]:

$$d\alpha/dt = K(T)f(\alpha) \qquad (2)$$

The value of K (reaction rate constant)has been calculated by the equation of Arrhenius:

$$K = Ae^{-E/RT} \qquad (3)$$

Where R is the gas constant, E is the activation energy and A is the pre-exponential factor. Substituting Eq. (3) into Eq. (2), we get:

$$d\alpha/dt = A\left(e^{-\frac{E}{RT}}\right)f(\alpha) \qquad (4)$$

When the temperature varied by a constant and controlled heating rate, Φ=dT/dt, the change in degree of conversion which is basically of temperature dependent becomes also time of heating dependent. Therefore Eq. (4) becomes:

$$d\alpha/dt = A/\emptyset\left(e^{-\frac{E}{RT}}\right)f(\alpha) \qquad (5)$$

The integrated result of Eq. (5) is mostly expressed as:

$$g(\alpha) = \int_0^{\alpha} \frac{d\alpha}{f(\alpha)} = A/\emptyset \int_0^{I} e^{-E/RT}\, dt \qquad (6)$$

where$g(\alpha)$ is the integrated result of the conversion dependence function. The right-hand side integral of Eq. (6) is known as temperature integral and has no closed form solution. The most used methods for evaluation of temperature integral are method of (CR) Fig. 7[37]and the approximation method of (HM)Fig.8[38]. From the results obtained, the following remarks can be pointed out:

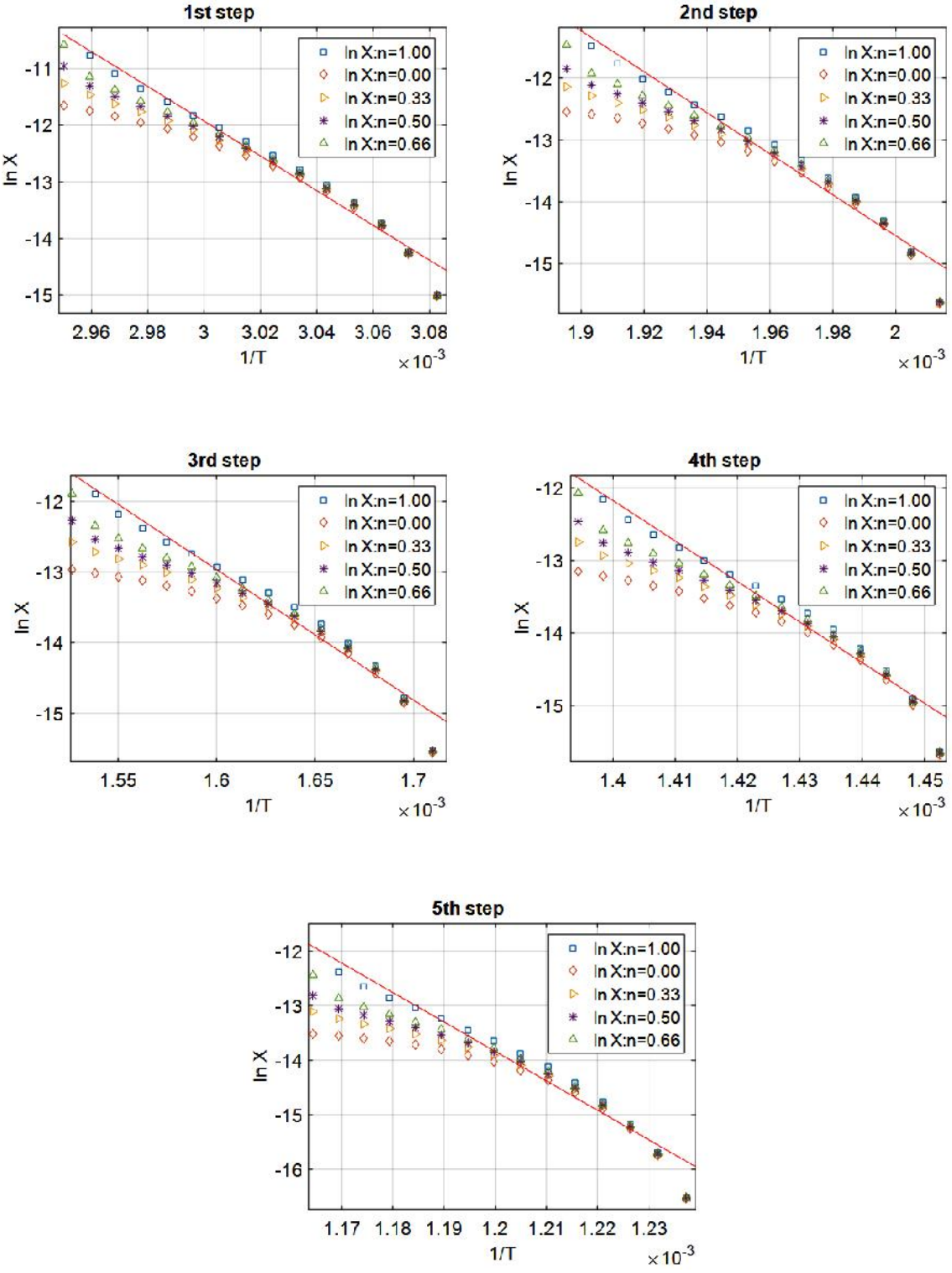

Figure 7: CR plots of [Co(IPT)Cl].H_2O complex.

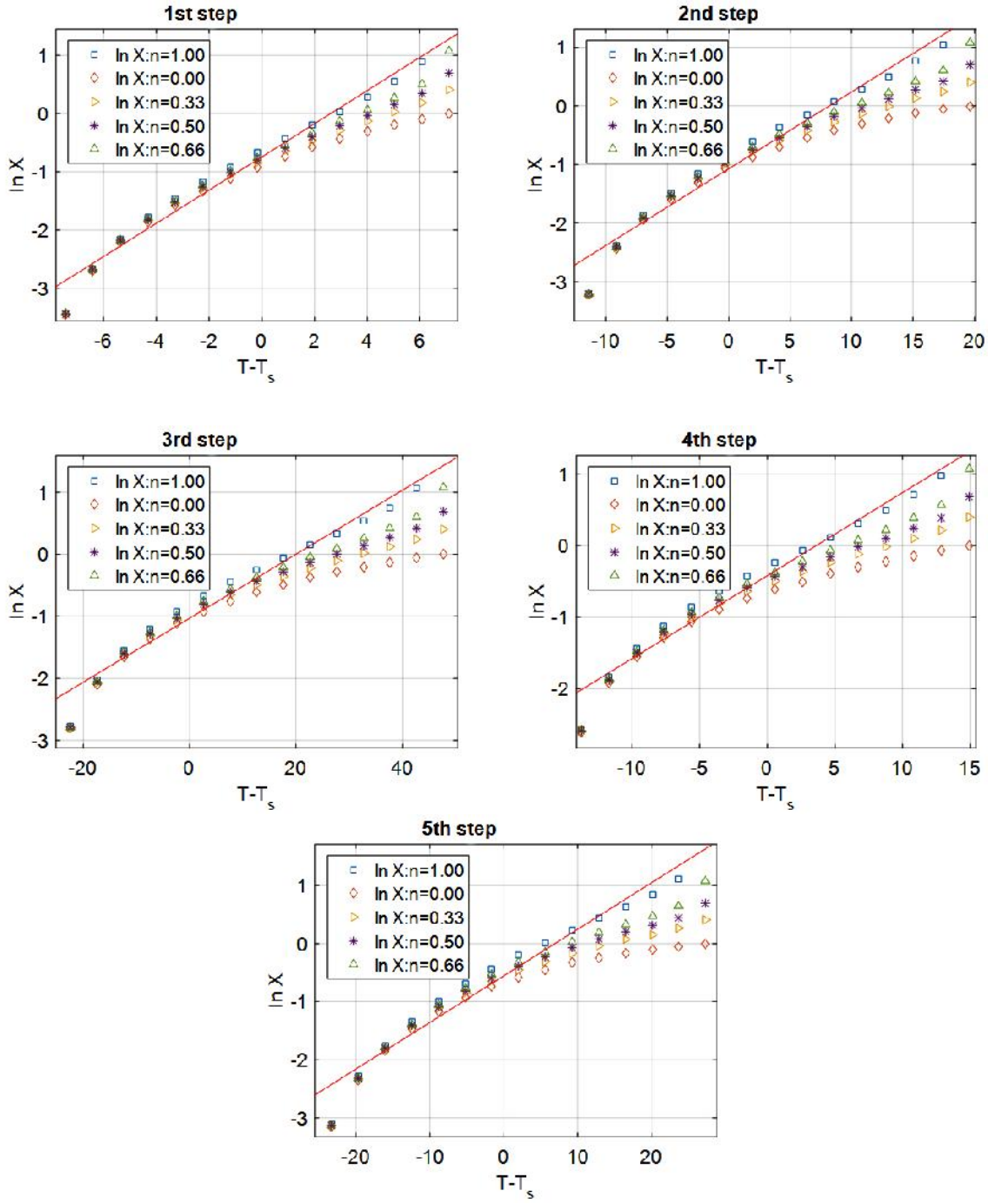

Figure 8: HM plots of [Co(IPT)Cl].H_2O complex.

(i) The kinetic parameters (E, A, ΔH, ΔS and ΔG) of all prepared solid complexes have been calculated by CR and HM method (Table 5). The outcomes obtained from the two models are quite comparable.

(ii) Only the degradation steps which show a best fit for (n=1) suggesting a decomposition of first- order in all cases. Other n values (eq.4 and 5) did not lead to better correlations.

(iii) The value of ΔG increases because the value of TΔS significantly from one stage to another which overrides the value of ΔH. Increasing the value of ΔG of a given complex on going from one decomposition step to another displayed that the rate of HIPT removal will be lower from step to the subsequent step [39, 40]. This lowering may be occurred because the oversize structural rigidity of remaining complex after the removal of one or more HIPT.

(iv) The values of the entropy of activation, ΔS* of the decomposition steps of the metal complexes indicate that the activated fragments have more ordered (negative values) or disordered (positive values) structure than the undecomposed complexes and/or the decomposition reactions are slow [37].

(v) The positive value of ΔH means the endothermic nature of the decomposition processes.

Table 5. Kinetic Parameters evaluated by CR and HM equations for the prepared complexes.

Compound	step	Mid Temp.(K)	Method	E_a KJ\mol	A (S^{-1})	ΔH* KJ\mol	ΔS* KJ\mol.K	ΔG* KJ\mol
[Co(IPT)Cl].H_2O	1st	331.85	HM	261.08	2.82×10^{39}	258.32	0.5094	89.27
			CR	254.78	2.90×10^{38}	252.02	0.4905	89.23
	2nd	507.94	HM	280.52	5.28×10^{26}	276.29	0.2622	143.09
			CR	275.89	1.82×10^{26}	271.66	0.2534	142.96
	3rd	607.33	HM	158.13	1.22×10^{11}	153.08	-0.0386	176.50
			CR	153.54	5.24×10^{10}	148.49	-0.0456	176.19
	4th	702.24	HM	476.25	3.40×10^{33}	470.41	0.3899	196.61
			CR	464.55	4.64×10^{32}	458.71	0.3733	196.54
	5th	831.47	HM	460.66	6.69×10^{26}	453.75	0.2601	237.47
			CR	448.11	1.12×10^{26}	441.20	0.2452	237.31
[Ni(IPT)$_2$]	1st	545.64	HM	462.15	1.70×10^{42}	457.62	0.5585	152.85
			CR	459.37	9.43×10^{41}	454.84	0.5536	152.76
	2nd	627.68	HM	221.22	1.16×10^{16}	216.00	0.0565	180.57
			CR	214.95	3.65×10^{15}	209.73	0.0468	180.34
	3rd	744.29	HM	447.20	5.98×10^{28}	441.02	0.2984	218.93
			CR	452.25	1.39×10^{29}	446.07	0.3054	218.76
[Cu(HIPT)Cl$_2$(H_2O)].H_2O	1st	401.20	HM	187.56	1.09×10^{22}	184.23	0.1745	114.20
			CR	188.64	1.57×10^{22}	185.30	0.1775	114.07
	2nd	450.01	HM	261.69	2.03×10^{28}	257.95	0.2936	125.82
			CR	258.35	8.57×10^{27}	254.61	0.2864	125.72
	3rd	509.73	HM	239.55	1.52×10^{22}	235.31	0.1753	145.95
			CR	238.91	1.36×10^{22}	234.67	0.1744	145.79
	4th	588.81	HM	212.39	2.97×10^{16}	207.49	0.0648	169.34
			CR	209.46	1.71×10^{16}	204.56	0.0602	169.12
	5th	674.63	HM	621.10	1.49×10^{46}	615.49	0.6323	188.95
			CR	614.11	4.36×10^{45}	608.50	0.6220	188.86
	6th	875.73	HM	215.77	1.80×10^{10}	208.49	-0.0576	258.90
			CR	205.19	$4.46\times10^{0}9$	197.91	-0.0691	258.46

Generally, there is reversible relation between the stepwise stability constants and the number of atoms of HIPT bonded to the metal ion [41, 42] therefore an inverse effect may occur during the decomposition process. Hence the rate of removal of the remaining HIPT will be less than that of the rate before the explosion of HIPT.

Molecular Modeling.

The molecular structure along with atom numbering of HIPTand its metal complexes are shown in Structures (2- 5).From the analysis of the data calculated for the bond lengths and angles, one can conclude the following:

i.The bond angles of the hydrazone moiety of HIPT were changed slightly upon coordination; the largest change affects in HIPT are C(21)-C(16)-N(17), C(16)-N(15)-C(13), S(14)-C(13)-N(12), C(21)-C(16)-N(15), N(15)-C(13)-S(14), C(13)-N(12)-N(11), N(17)-C(16)-N(15), N(15)-C(13)-N(12) and N(12)-N(11)-C(7) angles. The bond angles in the HIPT are diminished or augmented on complex formation as a result of bonding **[43]**.

ii. The bond angles are very near to an octahedral geometry expectingd^{2}sp^3 or sp^{3}d^2 hybridization in complexes of Ni(II), and Cu(II) metal ion. On the other hand, Co(II) complex afforded a tetrahedral geometry with sp^3 hybridization[37].

iii. All the active groups in taking part in coordination have bonds longer than that already exist in the ligand moiety like (C=O), (C-O)$_{phenolic}$, C=N$_{azomethine}$, C=N$_{pyridine}$ and C=SThis is referred to the formation of the M-N bond which makes the C-N bond weaker as a result of coordination via N atom of (C=N)$_{azomethine}$and (C=N)$_{pyridine}$**[44]**

iv. The complexation make the bond lengths of C(13)-N(12) and C(7)-N(11) shorter than of HIPT as the coordination takes place via N atoms of -C=N-C=N- group that is formed on deprotonation of SH group in all complexes **[43]** except in Cu(II) complex will becomes slightly longer due to coordination take places without enolization. This is referred to the formation of the M-N bond as a result of coordination via N atom of (C=N)$_{az}$**[44]**.

v. The bond angles of ligand moiety containing atoms of coordination will be changed in all respective compounds because the formation of N-M–S chelate ring **[45]**.

vi. According to the order of M-N$_{azomethine}$, M-N$_{pyridine}$ and M-S bond lengths, the data show the high strength of the Co-N and Co-S bonds.

vii. The energy values of both HOMO (π donor) and LUMO (π acceptor) are important parameters in quantum calculations Fig.9.

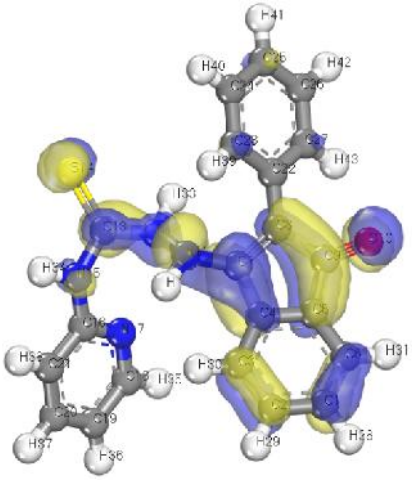

E_{LUMO}= -3.171*eV*
(excited state)

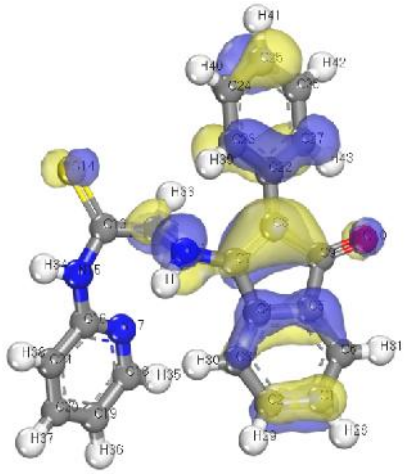

$E_{HOMO=}$ -4.538*eV*
(ground state)

Fig 9. 3D plots frontier orbital energies using DFT method for HIPT.

In many reactions, the nearby belong to HOMO and LUMO orbitals considered as a control factor, where in HIPT; the orbitals of higher molecular coefficients can be considered as the basic centers of bonding. The energy gap (E_{HOMO} -E_{LUMO}) is a significant stability index facilitate the characterization of both kinetic stability and chemical reactivity of the molecules[46]. Molecules with a tiny gap are considered soft molecules, they are highly polarized and more reactive than hard ones because they easily offer electrons to an acceptor. In Cu(II) complex, the energy gap is tiny showing that charge transfers easily in it and this affected the biological potency of the molecule. Moreover, the low amount of energy gap is because some groups enter into conjugation [47].

DFT method sites the selectivity of the molecular systems and concepts the chemical reactivity. The energies of frontier molecular orbitals (E_{HOMO}, E_{LUMO}), electro negativity (χ), energy band gap which explains the eventual charge transfer interaction within the molecule, global hardness (η), chemical potential (μ), global electrophilicity index (ω)and global softness (S) [48, 49] are listed in Table 6.

$\chi = -1/2\ (E_{LUMO} + E_{HOMO})$ (7)
$\mu = -\chi = 1/2\ (E_{LUMO} + E_{HOMO})$ (8)
$\eta = 1/2\ (E_{LUMO} - E_{HOMO})$ (9)
$S = 1/2\ \eta$ (10)
$\omega = \mu^2/2\ \eta$ (11)
The inverse value of the global hardness is designed as the softness ϭ as follow:
$\sigma = 1/\eta$ (12)

Table 6. Calculated E_{HOMO}, E_{LUMO}, energy band gap ($E_H - E_L$), chemical potential (μ), electronegativity (χ), global hardness (η), global softness (S) and global electrophilicity index (ω) for HIPT and its complexes.

Compound	E_H (eV)	E_L (eV)	(E_H-E_L) (eV)	χ (eV)	μ(eV)	η (eV)	S (eV^{-1})	ω(eV)	Ϭ (eV)
HIPT	-4.538	-3.171	-1.367	3.855	-3.855	0.684	0.342	10.868	1.463
[Co(IPT)Cl].H_2O	-4.203	-3.070	-1.133	3.637	-3.637	0.567	0.283	11.672	1.765
[Ni$(IPT)_2$]	-4.010	-3.508	-0.502	3.759	-3.759	0.251	0.126	28.148	3.984
[Cu(HIPT)Cl_2(H_2O)].H_2O	-4.947	-3.421	-1.526	4.184	-4.184	0.763	0.382	11.472	1.311

Biological Activity

Antimicrobial activity

Metal complexes of HIPT ligand were tested against *E. coli* as Gram –ve bacteria, *staphylococcus aureus (St. A.);* as Gram +ve bacteria organisms and comparison of inhibition zone (in mm) of metal complexes against *Candida albicans* are shown in fig. 10.

Degree of effectiveness was measured by determining the diameters of the zone of inhibition caused by the compounds. Effectiveness was classified into three zones on the bases of their diameter of zone of inhibition as shown in table 7.

The compounds were explained against both gram (-) negative, gram (+) positive bacteria and *C. albicans* on the basis of the results presented as given below and shown.

> 65%	Most effective
>35 to 65%	Moderate effective
>0 to 35%	Slightly effective
0%	Non effective

From fig .10, the following remarks on metal complexes will be obtained:

i. The slightly effect against *E. coli* was presented in Cu(II) complex.

ii. Cu(II) and Ni(II) complexes of HIPT are slightly effective against *S. aureus*

iii. Co(II) complex of (HIPT) is non-effective against all organisms.

Increased activity of complexes has been explained on its foundation of overtone concept and chelation theory. According to chelation, polarity of metal ion was reduced largely owing to overlap of ligand orbital and partial sharing of positive charge of metal with donor groups and so that the increases delocalization of electrons over completely chelate ring and consequently enhancement of lipophilicity of complex. So the enhancement of penetration of complex into lipid membrane and break down metal binding sites on enzymes of microorganism. Negative observations can be attributed either to inability of complexes to diffuse into cell wall of bacterium and hence cannot be interfere with their biological activity or they can diffuse and inactivated by unknown cellular mechanism i.e. bacterial enzymes.

Table 7: Activity index of complexes of HIPT on *E. coli*, *S. aureus* and *C. albicans.*

Compound	*E. coli* (mg/ml)		*S. aureus* (mg/ml)		*C. albicans* (mg/ml)	
	Diameter of inhibition zone (in mm)	**% Activity index**	**Diameter of inhibition zone (in mm)**	**% Activity index**	**Diameter of inhibition zone (in mm)**	**% Activity index**
$[Co(IPT)Cl].H_2O$	NA	----	NA	----	NA	----
$[Cu(HIPT)Cl_2(H_2O)].H_2O$	5	20.8	7	31.8	NA	----
$[Ni(IPT)_2]$	NA	----	4	18.2	NA	----
Ampicillin	24	100	22	100	NA	----
Colitrimazole	NA	----	NA	----	26	100

- NA→ No Activity.

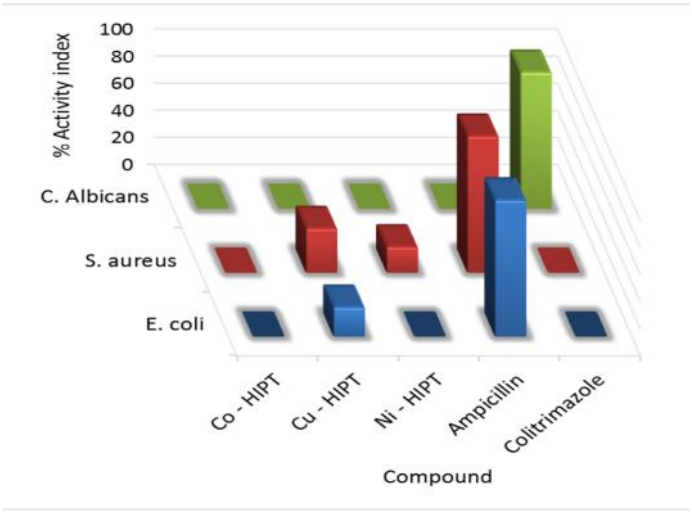

Figure 10: Comparison of activity index (%) of complexes of HIPT ligand against Gram-negative, Gram-positive bacterial stains and *C. albicans*.

Antioxidant Activity by ABTS method:

Even under optimal circumstances, reactive oxygen species (ROS),including ($O^{\cdot -}_2$), the ($\cdot OH$) and (H_2O_2) produced as a byproduct of normal metabolism in different subcellular compartments [50]. Also, ROS are produced during periods of development and at hard stresses. Moreover, ROS produced as a result of the hypersensitive response to pathogen infection. The ROS can damage DNA, proteins, membrane functions, generate lipid peroxidation may be responsible of human diseases, such as cancer, diabetic mellitus, hypertension and aging [51]. To inhibit treatment and repair damage initiated by ROS, cells have developed a complex antioxidant system [52].

The antioxidant efficiancy assay [53]depends on measuring the consumption of stable free radicals. The methodology assumes that the consumption of the stable free radical (X') will be determined by reactions as follows:

$$X' + YH \rightarrow XH + Y'$$

The rate and / or the extent of the process measured in terms of the decrease in X' concentration, would be related to the ability of the added compounds to trap free radicals. The decrease in color intensity of the free radical solution due to scavenging of the free radical by the antioxidant material is measured colorimetry at a specific wavelength.

Inhibition free radical ABTS in percent (I %) was calculated as in Eq:

$$I\% = (A_{blank} - A_{sample}) / (A_{blank}) \times 100$$

Where A_{blank} is the absorbance of the control reaction (containing all reagents except the test compound), and A_{sample} is the absorbance of the test sample.

The advantage of ABTS-derived free radical method over other methods is that the produced color remains stable for than one hour and the reaction is stoichiometric. All compounds were tested for antioxidant activity using ABTS assay. An inspection to the data in table 8 and figure 11 indicates that Co(II) and Ni(II) complexes proved to exhibit potent antioxidative activity. On the other hand, Cu(II) complex exhibited very weak antioxidant activity.

Table 8: ABTS scavenging activity of metal complexes of HIPT.

Compound	Absorbance	ABTS Inhibition (%)
Control of ABTS	0.525	0
Ascorbic acid	0.059	88.4
$[Co(IPT)Cl].H_2O$	0.080	84.3
$[Cu(HIPT)Cl_2(H_2O)].H_2O$	0.413	19.0
$[Ni(IPT)_2]$	0.085	83.3

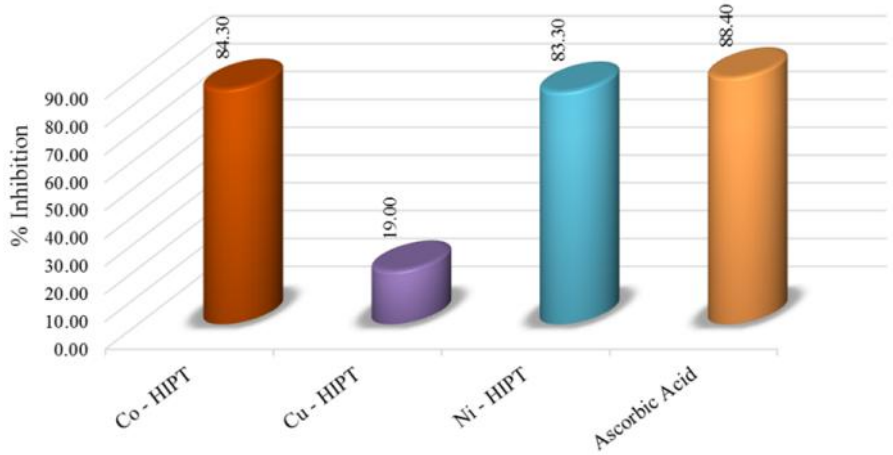

Figure 11: ABTS scavenging activity of complexes of HIPT.

Cytotoxicity assay

In our experiments, IC_{50} values (compound concentration that produces 50% of cell death) in micro molar units were calculated. For comparison purposes the cytotoxicity of Fluorouracil (5-FU) and the free ligand as well as its complexes has been evaluated under the same experimental conditions. It is clearly observed that chelation with metal has no synergistic effect on the cytotoxicity. Importantly, it should be emphasized that Ni(II) complex show moderate activity related to that of Fluorouracil (21.8 µg/ml) for (HePG-2). While Co(II) complex moderate activity (23.5 µg/ml) for (PC-3). These gratifying results are encouraging its further screening in vitro. Later on, upon further analysis, these complexes also exhibit considerable cell growth inhibition activity against human liver hepatocellular carcinoma (HePG-2) and human prostate cancer cell line (PC-3). Therefore, its further biological evaluation in vivo as well as studies of mechanism of action is necessary [54].

From table 9, the tested human tumor cells of hepatocellular carcinoma (HePG-2) and human prostate cancer cell line (PC-3) [figs .12 and 13] against the complexes of HIPT, Show moderate response of the Co(II) and Ni(II) complexes towards both cell line (HePG-2 and PC-3). While the weak activity was appeared in Cu(II) complex against HePG-2 cell line. But non-cytotoxic activity for (PC-3) is showed in Cu(II) complex.

Table 9: *In vitro* Cytotoxicity IC_{50} activity of HIPT-complexes against human tumor cells.

Compound	*In vitro* Cytotoxicity IC_{50} (µg/ml)	
	HePG-2	PC-3
5-Fluorouracil	6.8±0.14	4.7±0.11
$[Co(IPT)Cl].H_2O$	29.5±1.04	23.5±1.07
$[Cu(HIPT)Cl_2(H_2O)].H_2O$	92.7±5.37	>100
$[Ni(IPT)_2]$	21.8±1.68	30.2±3.35

• 5-FU: 5-fluorouracil.
• IC50 (µg/ml): 1 – 10 (very strong). 11 – 20 (strong). 21 – 50 (moderate). 51 – 100 (weak) and above 100 (non-cytotoxic)

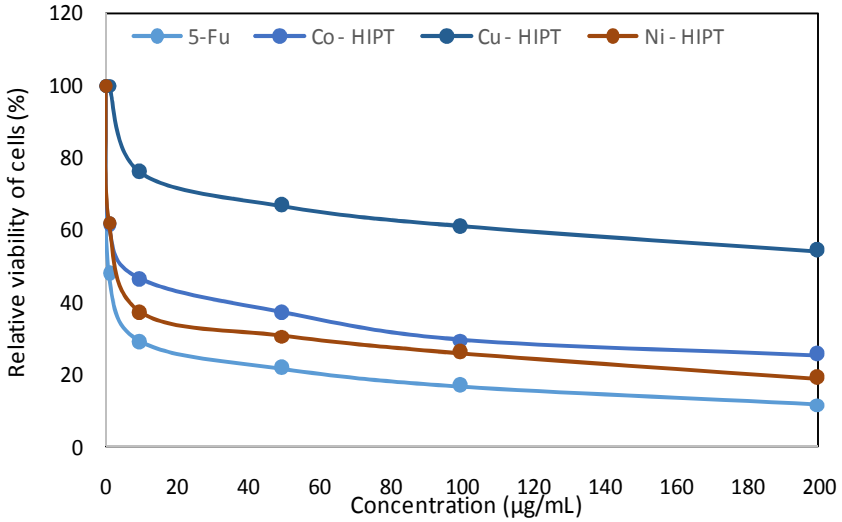

Figure12: Relative viability of tumor cells (HePG-2) with concentration of HIPT-complexes.

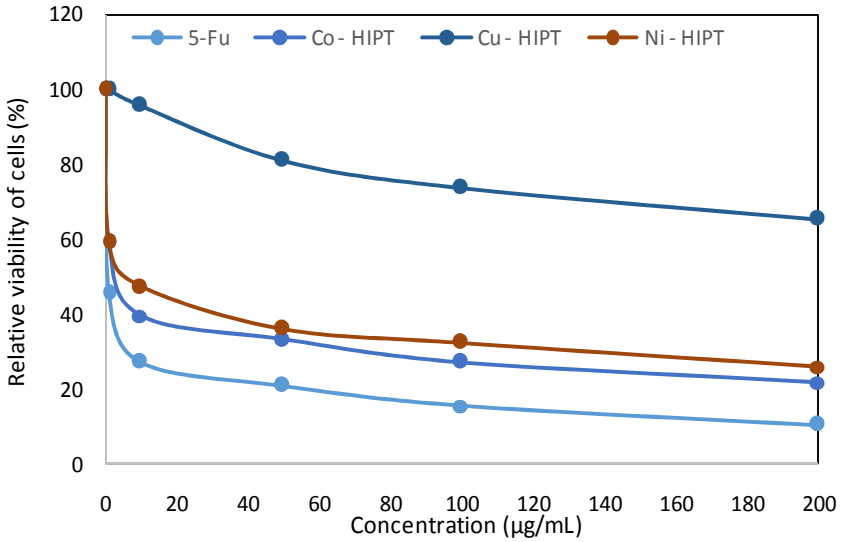

Figure 13: Relative viability of tumor cells (PC-3) with concentration of HIPT-complexes.

Conclusion

The hydrazone derived from the condensation of 4-(2-pyridyl)-3-thiosemicarbazide in a 1:1 molar ratio with 2-phenyl-1H-indene-1,3(2H)-dione and its Co(II), Ni(II) and Cu(II) complexes were prepared.IR spectra suggest that the HIPT coordinates as neutral tridentate ligand in Cu(II) complex. While, it behaves in Co(II) and Ni(II) complexes as mono-negative tridentate. The thermal decomposition behaviour was discussed and Kinetic parameters of resulted thermal decomposition stages have been calculated using Coats-Redfern and Horowitz-Metzger methods.The proposed geometries of isolated complexes were proved using DFT. Co(II) complex shows potent antioxidant activity and moderate Cytotoxicity activity. On the other hand, Co(II) complex has no activity against *Staphylococcus aureus, Escherichia coli* and *Candida albicans.*

References

[1] Yousef, T., El-Gammal, O., Ghazy, S., and Abu El-Reash, G. 2011. Synthesis, spectroscopic characterization, pH-metric and thermal behavior on Co (II) complexes formed with 4-(2-pyridyl)-3-thiosemicarbazide derivatives, *J. Mol. Struct.1004*, 271-283.

[2] Kaushik, N., and Mishra, A. 2003. Synthesis, characterization and thermal studies of some new organotin (IV) complexes with aniline N-thiohydrazide and benzaldehyde aniline N-thiohydrazone, *indian Journal of Chemistry Section A42*, 2762-2766.

[3] Dede, B., Karipcin, F., and Cengiz, M. 2009. Novel homo-and hetero-nuclear copper (II) complexes of tetradentate Schiff bases: Synthesis, characterization, solvent-extraction and catalase-like activity studies, *J. Hazard. Mater.163*, 1148-1156.

[4] Mishra, A., Manav, N., and Kaushik, N. 2005. Organotin (IV) complexes of thiohydrazones: synthesis, characterization and antifungal study, *Spectrochimica Acta Part A: Molecular and Biomolecular Spectroscopy61*, 3097-3101.

[5] Abd El Wahed, M., Nour, E., Teleb, S., and Fahim, S. 2004. Thermodynamic and thermal investigation of Co (II), Ni (II) and Cu (II) complexes with adenine, *J. Therm. Anal. Calorim.76*, 343-348.

[6] West, D. X., Padhye, S. B., and Sonawane, P. B. 1991. Structural and physical correlations in the biological properties of transition metal heterocyclic thiosemicarbazone and S-alkyldithiocarbazate complexes, In *Complex Chemistry*, pp 1-50, Springer.

[7] Padhye, S., and Kauffman, G. B. 1985. Transition metal complexes of semicarbazones and thiosemicarbazones, *Coord. Chem. Rev.63*, 127-160.

[8] Campbell, M. J. 1975. Transition metal complexes of thiosemicarbazide and thiosemicarbazones, *Coord. Chem. Rev.15*, 279-319.

[9] Omar, A., Mohsen, M., Labouta, I. M., Kasem, M. G., and Bourdais, J. 1983. Arylidenepyruvic acid thiosemicarbazone and thiazoline derivatives as potential antimicrobial agents, *J. Pharm. Sci.72*, 1226-1228.

[10] Klayman, D., Bartosevich, J., Griffin, T., Mason, C., and Scovill, J. P. 1979. *J. Med. Chem.22*, 885.

[11] Blanz, E. J., and French, F. A. 1968. The carcinostatic activity of 5-hydroxy-2-formylpyridine thiosemicarbazone, *Cancer Res.28*, 2419-2422.

[12] Miller 3rd, M., Stineman, C., Vance, J., West, D., and Hall, I. 1997. The cytotoxicity of copper (II) complexes of 2-acetyl-pyridyl-4N-substituted thiosemicarbazones, *Anticancer Res.18*, 4131-4139.

[13] Miller, M., Stineman, C., Vance, J., West, D., and Hall, I. 1999. Multiple mechanisms for cytotoxicity induced by copper (II) complexes of 2-acetylpyrazine-N-substituted thiosemicarbazones, *Appl. Organomet. Chem.13*, 9-19.

[14] Scovill, J. P., Klayman, D. L., Lambros, C., Childs, G. E., and Notsch, J. D. 1984. 2-Acetylpyridine thiosemicarbazones. 9. Derivatives of 2-acetylpyridine 1-oxide as potential antimalarial agents, *J. Med. Chem.27*, 87-91.

[15] Vogel, A. I. 1991. *Vogel'sTextbook of Quantitative Chemical Analysis*, 5th ed., Longmans, London.

[16] Yousef, T. A., Badria, F. A., Ghazy, S. E., El-Gammal, O. A., and El-Reash, G. M. A. 2011. In vitro and in vivo antitumor activity of some synthesized 4-(2-pyridyl)-3-Thiosemicarbazides derivatives, *International Journal of Medicine and Medical Sciences3*, 37-46.

[17] Stylianakis, I., Kolocouris, A., Kolocouris, N., Fytas, G., Foscolos, G. B., Padalko, E., Neyts, J., and De Clercq, E. 2003. Spiro [pyrrolidine-2, 2′-adamantanes]: synthesis, anti-influenza virus activity and conformational properties, *Bioorg. Med. Chem. Lett.13*, 1699-1703.

[18] Lissi, E. A., Modak, B., Torres, R., Escobar, J., and Urzua, A. 1999. Total antioxidant potential of resinous exudates from Heliotropium species, and a comparison of the ABTS and DPPH methods, *Free Radical Res.30*, 471-477.

[19] El-Gazzar, A., Youssef, M., Youssef, A., Abu-Hashem, A., and Badria, F. 2009. Design and synthesis of azolopyrimidoquinolines, pyrimidoquinazolines as anti-oxidant, anti-inflammatory and analgesic activities, *Eur. J. Med. Chem.44*, 609-624.

[20] Aeschbach, R., Löliger, J., Scott, B. C., Murcia, A., Butler, J., Halliwell, B., and Aruoma, O. I. 1994. Antioxidant actions of thymol, carvacrol, 6-gingerol, zingerone and hydroxytyrosol, *Food Chem. Toxicol.32*, 31-36.

[21] Mosmann, T. 1983. Rapid colorimetric assay for cellular growth and survival: application to proliferation and cytotoxicity assays, *J. Immunol. Methods65*, 55-63.

[22] Mauceri, H. J., Hanna, N. N., Beckett, M. A., Gorski, D. H., Staba, M.-J., Stellato, K. A., Bigelow, K., Heimann, R., Gately, S., and Dhanabal, M. 1998. Combined effects of angiostatin and ionizing radiation in antitumour therapy, *Nature394*, 287-291.

[23] Delley, B. 2002. Hardness conserving semilocal pseudopotentials, *Phys. Rev. B: Condens. Matter66*, 155125.

[24] Modeling and Simulation Solutions for Chemicals and Materials Research, Materials Studio, *Version 7.0*, Accelrys software Inc., San Diego, USA (2011).

[25] Hehre, W. J. 1986. *Ab initio molecular orbital theory*, Wiley-Interscience.

[26] Kessi, A., and Delley, B. 1998. Density functional crystal vs. cluster models as applied to zeolites, *Int. J. Quantum Chem68*, 135-144.

[27] Matveev, A., Staufer, M., Mayer, M., and Rösch, N. 1999. Density functional study of small molecules and transition-metal carbonyls using revised PBE functionals, *Int. J. Quantum Chem75*, 863-873.

[28] Hammer, B., Hansen, L. B., and Nørskov, J. K. 1999. Improved adsorption energetics within density-functional theory using revised Perdew-Burke-Ernzerhof functionals, *Phys. Rev. B: Condens. Matter59*, 7413-7421.

[29] Abdel-Wahab, B. F., Awad, G. E., and Badria, F. A. 2011. Synthesis, antimicrobial, antioxidant, anti-hemolytic and cytotoxic evaluation of new imidazole-based heterocycles, *Eur. J. Med. Chem.46*, 1505-1511.

[30] El-Gammal, O. A., El-Reash, G. A., and Ahmed, S. F. 2012. Structural, spectral, thermal and biological studies on 2-oxo-N′-((4-oxo-4H-chromen-3-yl) methylene)-2-(phenylamino) acetohydrazide (H 2 L) and its metal complexes, *J. Mol. Struct.1007*, 1-10.

[31] El-Gammal, O. A., El-Reash, G. M. A., and El-Gamil, M. M. 2014. Structural, spectral, pH-metric and biological studies on mercury (II), cadmium (II) and binuclear zinc (II) complexes of NS donor thiosemicarbazide ligand, *Spectrochimica Acta Part A: Molecular and Biomolecular Spectroscopy123*, 59-70.

[32] El-Gammal, O., El-Reash, G. A., and El-Gamil, M. 2012. Binuclear copper (II), cobalt (II) and Nickel (II) complexes of N 1-ethyl-N 2-(pyridin-2-yl) hydrazine-1, 2-bis (carbothioamide): Structural, spectral, pH-metric and biological studies, *Spectrochimica Acta Part A: Molecular and Biomolecular Spectroscopy96*, 444-455.

[33] El-Ayaan, U., Kenawy, I., and El-Reash, Y. A. 2007. Synthesis, thermal and spectral studies of first-row transition metal complexes with Girard-T reagent-based ligand, *J. Mol. Struct.871*, 14-23.

[34] El-Gammal, O. A., Abu El-Reash, G. M., and El-Gamil, M. M. 2012. Binuclear copper(II), cobalt(II) and Nickel(II) complexes of N1-ethyl-N2-(pyridin-2-yl) hydrazine-1,2-bis(carbothioamide): Structural, spectral, pH-metric and biological studies, *Spectrochimica Acta Part A: Molecular and Biomolecular Spectroscopy96*, 444-455.

[35] Singh, A., and Singh, P. 2000. Synthesis, characterization and antiinflammatory effects of Cr (III), Mn (II), Fe (III) and Zn (II) complexes with diclofenac sodium, *Indian J. Chem., Sect A39*, 874-876.

[36] Patil, R. M. 2007. Synthetic, structural and biological properties of binuclear complexes with some schiff bases, *Acta Pol. Pharm. Drug Res64*, 345-353.

[37] Moore, J. W., and Pearson, R. G. 1961. *Kinetics and mechanism*, John Wiley & Sons, New York.

[38] Hatakeyama, T., and Quinn, F. 1994. Fundamentals and applications to polymer science, *J. Therm. Anal.*

[39] Maravalli, P., and Goudar, T. 1999. Thermal and spectral studies of 3-N-methyl-morpholino-4-amino-5-mercapto-1, 2, 4-triazole and 3-N-methyl-piperidino-4-amino-5-mercapto-1, 2, 4-triazole complexes of cobalt (II), nickel (II) and copper (II), *Thermochim. Acta325*, 35-41.

[40] Yusuff, K. M., and Sreekala, R. 1990. Thermal and spectral studies of 1-benzyl-2-phenylbenzimidazole complexes of cobalt (II), *Thermochim. Acta159*, 357-368.

[41] Siddalingaiah, A. H. M., and Naik, S. G. 2002. Spectroscopic and thermogravimetric studies on Ni(II), Cu(II) and Zn(II) complexes of di(2,6-dichlorophenyl)carbazone, *J. Mol. Struct. THEOCHEM582*, 129-136.

[42] Chacko, J., and Parameswaran, G. 1984. Thermal decomposition kinetics of vanillidene anthranilic acid complexes of cobalt (II), nickel (II), copper (II) and zinc (II), *J. Therm. Anal. Calorim.29*, 3-11.

[43] El-Gammal, O. A. 2010. Synthesis, characterization, molecular modeling and antimicrobial activity of 2-(2-(ethylcarbamothioyl) hydrazinyl)-2-oxo-N-phenylacetamide copper complexes, *Spectrochimica Acta Part A: Molecular and Biomolecular Spectroscopy75*, 533-542.

[44] Despaigne, A. A. R., Da Silva, J. G., Do Carmo, A. C. M., Piro, O. E., Castellano, E. E., and Beraldo, H. 2009. Copper (II) and zinc (II) complexes with 2-benzoylpyridine-methyl hydrazone, *J. Mol. Struct.920*, 97-102.

[45] El-Gammal, O., Bekheit, M., and Tahoon, M. 2015. Synthesis, characterization and biological activity of 2-acetylpyridine-α-naphthoxyacetylhydrazone its metal complexes, *Spectrochimica Acta Part A: Molecular and Biomolecular Spectroscopy135*, 597-607.

[46] Govindarajan, M., Periandy, S., and Carthigayen, K. 2012. FT-IR and FT-Raman spectra, thermo dynamical behavior, HOMO and LUMO, UV, NLO properties, computed frequency estimation analysis and electronic structure calculations on α-bromotoluene, *Spectrochim. Acta. A Mol. Biomol. Spectrosc.97*, 411-422.

[47] Abu El-Reash, G. M., El-Gammal, O., Ghazy, S., and Radwan, A. 2013. Characterization and biological studies on Co (II), Ni (II) and Cu (II) complexes of carbohydrazones ending by pyridyl ring, *Spectrochim. Acta. A Mol. Biomol. Spectrosc.104*, 26-34.

[48] Pearson, R. G. 1989. Absolute electronegativity and hardness: applications to organic chemistry, *J. Org. Chem.54*, 1423-1430.

[49] Padmanabhan, J., Parthasarathi, R., Subramanian, V., and Chattaraj, P. 2007. Electrophilicity-based charge transfer descriptor, *J. Phys. Chem. A111*, 1358-1361.

[50] Fujisawa, K., Kakizaki, T., Miyashita, Y., and Okamoto, K.-i. 2008. Structural and spectroscopic comparison of five-coordinate cobalt(II) and nickel(II) thiolato complexes with the related four-coordinate complexes, *Inorg. Chim. Acta361*, 1134-1141.

[51] Rao, C. N. R., and Venkataraghavan, R. 1962. *Spectrochim. Acta A18*, 541.

[52] Beynon, J. H. 1960. *Mass Spectrometry and its Applications to Organic Chemistry*, Elsevier, Amsterdam.

[53] Aliage, C., and Lissi, E. A. 1998. *Int. J. Chem. Kinet.30*, 565-570.

[54] Yousef, T., El-Reash, G. A., El-Gammal, O., and Ahmed, S. F. 2014. Structural, DFT and biological studies on Cu (II) complexes of semi and thiosemicarbazide ligands derived from diketo hydrazide, *Polyhedron81*, 749-763.

Access this Article in Online	
	Website: www.ijarbs.com
	Subject:
Quick Response Code	

How to cite this article:
Ola A. El-Gammal, Ibrahim M. El-Mehasseb, Raghda H. Salama, Gaber M. Abu El-Reash. (2016). Coordination behaviour and biological activity of Co(II), Ni(II) and Cu(II) complexes of phenyl indandionepyridyl thiosemicarbazone ligand.. Int. J. Adv. Res. Biol. Sci. 3(6): 263-282.